Tip Streaming from a Drop in the Presence of Surfactants

Charles D. Eggleton,[1] Tse-Min Tsai,[2] and Kathleen J. Stebe[3]

[1]*Department of Mechanical Engineering, UMBC, Baltimore, Maryland 21250*

[2]*School of Mechanical and Production Engineering, Nanyang Technological University, Singapore*

[3]*Department of Chemical Engineering, The Johns Hopkins University, 3400 North Charles Street, Baltimore, Maryland 21218*

(Received 5 April 2000; published 9 July 2001)

Drop breakup in a linear extensional flow is simulated numerically using a nonlinear model for the surface tension that accounts for maximum packing at the interface. Surface convection sweeps surfactant to the drop poles, where it accumulates and drives the surface tension to near zero. The drop assumes a transient shape with highly pointed tips. From these tips, thin liquid threads are pulled. Subsequently, small, surfactant-rich droplets are emitted from the termini of these threads. The scale of the shed drops depends on the initial surfactant coverage. Dilute initial coverage leads to tip streaming, while high initial coverage leads to the tip dropping breakup mode.

DOI: 10.1103/PhysRevLett.87.048302 PACS numbers: 83.50.Jf

Understanding the breakup of droplets under dynamic flow conditions is of practical significance when immiscible fluids must be dispersed in each other to create emulsions, and in understanding the stability and rheology of emulsions once formed. Surfactants are added to the fluid mixtures to reduce the surface tension, reducing the work required to create new interface. Under dynamic conditions, surfactants alter the interfacial stresses in a complex manner that depends on the surfactant mass transfer dynamics and the amount of surfactant adsorbed. As a result, surfactants can either resist or enhance drop deformation under flow. Surfactants can also cause droplets to break under flow which would be stable in their absence. In this note, surfactant-induced drop breakup is studied in a model flow field, that of a drop in a linear uniaxial extensional flow, as shown in Fig. 1.

We focus on a mode of drop breakup termed tip streaming, first seen by Taylor [1] over sixty years ago, but only recently linked to the presence of surfactants. As the tip streaming phenomenon occurs, daughter drops of a much smaller scale are ejected from thin threads formed at the drop poles. Tip streaming occurs at flow rates significantly below the critical flow rates for breakup of clean drops. After a finite number of daughter drops have been ejected, the parent drop can attain a stable shape. Drops in both extensional and shear flow have been observed to form highly pointed tips (cusps) from which a nearly continuous stream of daughter drops is ejected. This occurs only when the ratio of the internal to external viscosity $\lambda < 0.2$ [2–8]. In the absence of surfactants, there is generally good agreement between observed and predicted deformations and breakup modes [9]. For example, drops with clean interfaces fail to fragment while the linear extensional flow is in effect and are drawn into finer filaments with time. By deliberately adding surfactant to the bulk suspending fluid in a controlled manner, de Bruijn [5] demonstrated that tip streaming occurs only at dilute surfactant concentrations in a shear flow. The shed daughter drops had radii 2 orders of magnitude smaller than their parent drops and had significantly reduced surface tensions. Janssen and co-workers found the same was true in both shear [6] and hyperbolic planar flows [7], and, at high surfactant concentrations, observed another mode of breakup, tip dropping. In tip dropping, the daughter drops are larger and are ejected more intermittently. Experiments have established that surfactants play a role in tip streaming; however, it is difficult to measure dynamic surface tension on the interface of a tip streaming drop. Numerical simulation provides a detailed description of the transient drop behavior that is needed to uncover the interaction between the velocity field, the surfactant distribution, and the interfacial stresses to illuminate the mechanisms that determine drop breakup.

When a surfactant adsorbs to establish a surface concentration Γ, the surface tension γ reduces from its clean interface value γ_o. Thermodynamics dictates that the dependence $\gamma(\Gamma)$ is highly nonlinear for finite changes in surface tension. The primary mechanism behind this nonlinear dependence is entropic; because surfactant molecules occupy finite cross sectional areas, there is an upper bound to the surface concentration, Γ_∞. A surface equation of state which accounts for this effect is [10,11]

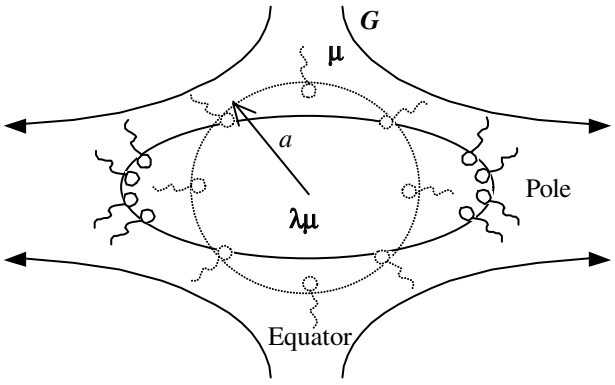

FIG. 1. Schematic of an initially spherical drop subjected to a uniaxial extensional flow.

$$\gamma = \gamma_o + RT\Gamma_\infty \ln(1 - \Gamma/\Gamma_\infty). \quad (1)$$

This equation adequately describes the behavior of a wide range of surfactants [12]. At equilibrium, it predicts that surface tension drops steeply as the fractional coverage of the interface (defined as $x = \Gamma_{\rm eq}/\Gamma_\infty$) approaches unity from below. However, it also predicts the unrealistic behavior that for some finite value of x, the surface tension can become negative. In the absence of flow, this unacceptable behavior is not realized for soluble surfactants. Initially, x increases in equilibrium with the bulk concentration of the surfactant, which is in solution in monomeric form at dilute concentrations. At some bulk concentration, however, surfactant monomers form aggregates (micelles) in solution, with the concentration of monomer in solution remaining fixed at the critical micelle concentration (CMC). The surface coverage remains at $x_{\rm CMC}$ in equilibrium with the surfactant monomer for all higher bulk concentrations. Since the surface tension in equilibrium with $x_{\rm CMC}$ is finite, in a quiescent system, $\gamma(x_{\rm CMC})$ provides a lower bound to the surface tension.

When the surfactant is present on a droplet in an imposed flow, the surfactant is swept toward the drop poles, where it can collect to concentrations in excess of those in equilibrium with the bulk solution. These nonequilibrium distributions are most pronounced at dilute bulk concentrations, for which the rates of surfactant exchange by adsorption desorption and bulk diffusion are so slow compared to the flow rate that the surfactant can be approximated as being insoluble. This limit is studied here. (See [13] for a detailed discussion.) In this circumstance, the surface tension can reduce to extremely low values. However, no lower bound on γ need be imposed. The surface tension remains finite because of the interplay of two mechanisms in the interfacial stress balance. (i) Regions of low tension deform to become increasingly curved to balance the normal stress jump, increasing the local area and diluting the interface. This is expressed in the Laplace pressure term, the product of the surface tension, and the mean curvature of the interface $2H$. (ii) Regions of high surface tension away from the drop poles contract strongly, exerting a stress that slows the tangential flux of surfactant toward the poles. This is the Marangoni stress, given by the negative surface gradient in the surface tension, $-\nabla_s\gamma = \frac{-\partial\gamma}{\partial\Gamma}\nabla_s\Gamma$. This stress increases very rapidly as x becomes finite, with a singularity that is of higher order than that in the surface tension. This strong tangential stress prevents the local accumulation of surfactant from becoming large enough to drive the surface tensions to zero. Including these two mechanisms, the stress balance at the interface is

$$[[p]]\mathbf{n} + [[\mathbf{n} \cdot \underline{\mathbf{T}}]] = -\frac{\partial\gamma}{\partial\Gamma}\nabla_s\Gamma + 2H\gamma\mathbf{n}, \quad (2)$$

where $\mathbf{n}$ is the surface normal, p is the pressure, $\underline{\mathbf{T}}$ is the viscous stress tensor, and the square brackets indicate jump quantities. In this work, the dissipative effects of surface viscosities, which are small for soluble surfactants, are neglected [14].

In our simulations, the deformation of a droplet is studied beginning from an initial state of a sphere of radius a with a uniform surfactant concentration $\Gamma_{\rm eq}$ and surface tension $\gamma_{\rm eq}$. Normalizing the surface tension with $\gamma_{\rm eq}$, the elasticity number $E = RT\Gamma_\infty/\gamma_{\rm eq}$ appears as a dimensionless number which couples the surface tension to the local surface concentration; this coupling is typically weak, and is set to 0.2 in our simulations. In the flow field of interest, the velocity obeys the imposed linear extensional flow far from the drop. The drop to suspending fluid viscosity ratio λ is fixed at 0.05. The velocities in the drop and external phases are governed by Stokes' equations; velocities are continuous at the interface and equal to the interfacial velocity $\mathbf{v}_s$. The shape of the drop is linked to the external flow field through the stress jump conditions at the interface, and the kinematic condition which requires that normal velocities be continuous across the drop interface. Defining the strain rate of the far field flow as G, and the viscosity of the suspending fluid as μ, the capillary number Ca can be defined as the ratio of the characteristic viscous stresses that deform the drop to the surface tension which resists deformation, ${\rm Ca} = (\mu G a)/\gamma_{\rm eq}$.

The external flow redistributes surfactant molecules and alters the local surfactant concentration according to a surface mass balance:

$$\frac{\partial\Gamma}{\partial t} + \nabla_s \cdot (\Gamma\mathbf{v}_t) + 2H\Gamma\mathbf{n} \cdot \mathbf{v}_n - D_s\nabla_s^2\Gamma = 0. \quad (3)$$

This balance requires that the rate of change in Γ be balanced by convective fluxes tangential to the interface, dilution by surface dilatation, and redistribution by surface diffusion. The surface diffusional flux is typically quite small. Recasting this equation in dimensionless form, the surface diffusion term goes as $({\rm Ca}\Lambda)^{-1}$, where $\Lambda = (\gamma_{\rm eq} a)/\mu D_s$; this latter dimensionless number is large for typical surfactant solutions. In our simulations, $\Lambda = 10^3\gamma_o/\gamma_{\rm eq}$.

The response of the drop is studied by numerically solving the Stokes' equations coupled with the mass balance equation and the surface equation of state. The boundary integral formulation of Stokes' equations in a quasistatic limit [15] is solved using standard techniques to obtain the interfacial velocity [16]. The drop interface is displaced according to the kinematic condition at each time step using a second order Runge-Kutta method. The time step was made proportional to the minimum surface tension. The mass balance equation is solved using standard second order finite difference approximations with an implicit time step. The convective term of the mass balance equation is discretized using an upwinding scheme to damp out oscillations when concentration gradients are large. The calculated steady state deformation of a clean drop as a function of viscosity ratio was compared to second order small deformation theory [17] for validation. For small

deformations (<0.15) the difference between theory and numerics is less than 2%. Strain rates under which the drop either attained a steady shape or continuously deformed with no stable shape were found by incrementing Ca from an initial value of 0.01. For a given value of Ca, a steady shape is found if the normal velocities everywhere along the interface approach zero. That steady shape is used as the initial condition for a new, higher value of Ca. The capillary number was increased in this manner for a drop with $\lambda = 0.05$ and a clean (or surfactant-free) interface; the last stable shape found for Ca = 0.095, while at Ca = 0.1 the drop was unstable and was continuously extended into a thinner thread by the external flow. Here we define the critical capillary number Ca_{cr} as the last value for Ca (in increments of 0.005) for which a stable shape could be realized, so $Ca_{cr} = 0.095$ for the clean drop. Tip streaming did not occur in a linear flow with a clean drop interface in either our simulations or in experiments performed with care to avoid surface active impurities [18].

Drop deformation was studied as a function of x for $\lambda = 0.05$; the deformations vary nonmonotonically with surfactant concentration in a manner similar to drops of unity viscosity ratio reported in [19], except that, because of the weak internal viscosity of the droplets in this case, surfactant was swept to the drop poles at all Ca studied, so the deformations were always greater than the clean interface case. The critical capillary number for stability, Ca_{cr} was also determined; it is compared to recent observations made in [20] on drops with $\lambda = 0.1$ in Fig. 2. Both the simulations and the measurements show a minimum in the critical capillary number over the range of surface tensions studied. In the simulations, for small x surfactant accumulates locally at the drop poles. As x increases, surfactant remains distributed over the drop, requiring stronger flows to drive breakup. Surfactant concentration at the drop poles becomes comparable to the maximum packing as Ca_{cr} is approached.

The effect of equilibrium surfactant concentration on the mode of drop breakup is studied for concentrations which were low ($x = 0.1$) and moderately high ($x = 0.75$). First, consider the case for $x = 0.1$, for which $Ca_{cr} = 0.06$. At this strain rate, surface convection has created a surfactant-free region of the interface near the drop equator and a surfactant-rich region near the drop pole (see left plot of Fig. 3), where the surface concentration and corresponding surface tension are $\Gamma_{\text{pole}} = 0.88\Gamma_\infty$ and $\gamma_{\text{pole}} = 0.59\gamma_o$, respectively. Incrementing the strain rate to Ca = 0.065, the interplay of the surfactant distribution, the surface tension and the unsteady evolution of the drop shape are studied. The surface tension evolution is shown in Fig. 3; the evolution of the drop shape is shown in Fig. 4. Surfactant accumulates near the drop pole, establishing a local concentration $\Gamma_{\text{pole}} > 0.99\Gamma_\infty$; this strongly reduces the surface tension to a value $\gamma_{\text{pole}} = 0.03\gamma_o$, and increases the local curvature to a maximum value of $2H_{\text{pole}} = 288$. The surface tension distribution for this instant in time is the dashed line in Fig. 3. Throughout this time period, surface tension in the equatorial region remains near the initial equilibrium value and provides a mechanism to resist deformation, while surface tension near the polar region of the drop is severely reduced, creating a small region near the pole that offers weak resistance to deformation.

As the simulation proceeds, a thin thread is pulled from the drop pole. As the thread is pulled, the interfacial area at the drop pole increases and surfactant concentration decreases from its maximum with a corresponding increase in surface tension (see right plot of Fig. 3). The curvature at the drop pole decreases from the maximum attained at the critical point as the thread is drawn further into the higher strain regions of the flow. As the surface tension decreases, the thread begins to neck. The thinning of this neck leads to formation of a daughter drop, shown in Fig. 4(b). The emitted daughter drop has an average surface tension of $0.51\gamma_o$ and volume of 1.325×10^{-4} (which would correspond to a sphere of radius 0.032). The ratio of daughter

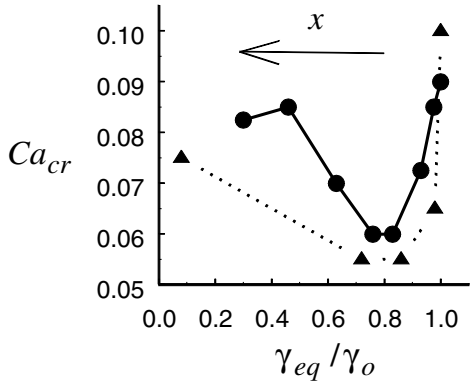

FIG. 2. Comparison of the critical capillary numbers for drop breakup, Ca_{cr}. (●) Experiment, $\lambda = 0.1$ [20]; (▲) simulation, $\lambda = 0.05$; $x = 0$, 0.1, 0.5, 0.75, and 0.99.

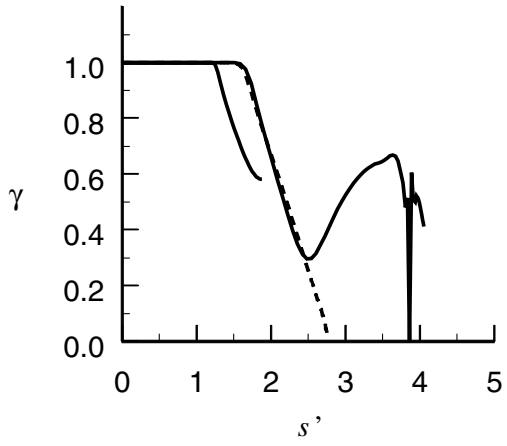

FIG. 3. Evolution in time (left to right) of the surface tension profile along the drop interface from the equator ($s' = 0$) to the drop pole. The surface tension decreases from nearly 1 at the equator and reaches a minimum of 0.03 (dashed line) before a jet is emitted from the drop pole.

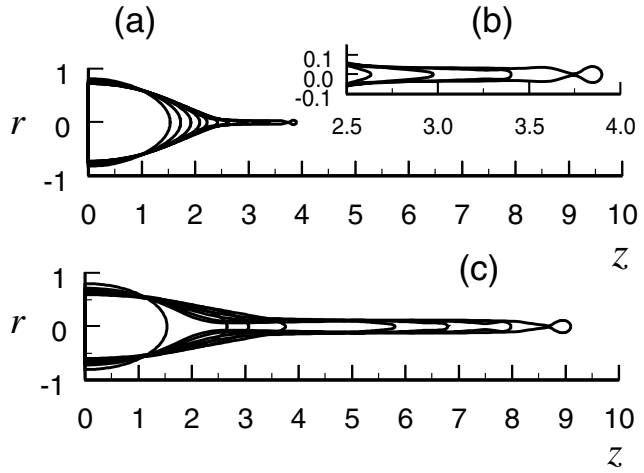

FIG. 4. (a) The evolution from a stable prolate spheroid to a drop undergoing tip streaming for $x = 0.1$ (b) A close-up of the droplet shed from the poles for $x = 0.1$. (c) The evolution from a stable prolate spheroid to a drop undergoing tip streaming for $x = 0.75$.

to parent radii is the same order of magnitude reported by de Bruijn in shear flow. Much of the surfactant is on the thin thread of average radius 0.03, while much of the parent drop interface is clean. Further emission of daughter drops provides a mechanism that leaves a cleaner parent drop that would be stable at this strain rate, as was observed in experiments.

The effect of a higher initial concentration on the mode of drop breakup is examined by simulating a drop with $x = 0.75$ with initial conditions provided by the stable drop at $\mathrm{Ca} = 0.05$ and incrementing the strain rate to $\mathrm{Ca} = 0.06$. Again, surfactant concentration at the drop pole approaches Γ_∞, followed by thread formation at the drop pole. The mechanisms that lead to jet and daughter drop emission are the same as the low coverage case; however, the thread and emitted drop are larger; see Fig. 4(c). The thread is pulled from the region near the pole where the surface tension is reduced, which covers far more of the drop at this higher initial concentration. The thread has an approximate radius of 0.10. The daughter drop has average surface tension $0.77\gamma_o$ and volume of 3.1×10^{-3}, corresponding to a sphere of radius 0.09. The thread also necks at the parent drop-thread juncture. If the drop were to snap off at this neck, the entire thread of volume 0.062, with corresponding radius 0.24, would form the much larger daughter drops of the tip dropping phenomenon [7,20].

Based on these simulations and experimental observations, we can begin to qualitatively describe the mechanisms that lead to the appearance and cessation of tip streaming as surfactant concentration is increased. For trace surface concentrations (well below $x = 0.1$), surface tension effects are negligible and the critical strain rate for a clean interface is reached before Γ_∞ is approached at the pole. The drop becomes unstable and extends as a continuous thread, with the possibility of surfactants altering the breakup of what already has become an unstable drop. At dilute concentrations (e.g., $x = 0.1$) convection drives surfactant towards the pole and Γ_∞ is approached at strain rates below the critical strain rate for the clean drop. Surface tension at the pole approaches (but does not reach) zero and sharp gradients in surface tension lead to the emission of a thread. These simulations and experiments [7,20] show that thread size increases with concentration. If significant surface tension gradients are present at high concentrations the thread diameter will be comparable to the parent drop diameter, leading to drop fracture. Current work focuses on studying the effect of extensional rate on thread diameter and closely examining the pressure and velocity fields surrounding the thread during daughter drop formation.

[1] G. I. Taylor, Proc. R. Soc. London A **146**, 501 (1934).
[2] W. Bartok and S. G. Mason, J. Colloid Sci. **14**, 13 (1959).
[3] F. D. Rumscheidt and S. G. Mason, J. Colloid Sci. **16**, 238 (1961).
[4] P. G. Smith and T. G. M. Van De Ven, Colloids Surf. **15**, 191 (1985).
[5] R. A. de Bruijn, Chem. Eng. Sci. **48**, 277 (1993).
[6] J. J. M. Janssen, A. Boon, and W. G. M. Agterof, AIChE. J. **40**, 1929 (1994).
[7] J. J. M. Janssen, A. Boon, and W. G. M. Agterof, AIChE. J. **43**, 1436–1447 (1997).
[8] D. C. Trethaway and L. G. Leal, AIChE. J. **45**, 929 (1999).
[9] H. A. Stone and L. G. Leal, J. Fluid Mech. **198**, 399 (1989).
[10] A. Frumkin, Kolloid Z. **116**, 466 (1925).
[11] R. Defay and I. Prigogine, *Surface Tension and Adsorption* (John Wiley and Sons, New York, 1966).
[12] C. H. Chang and E. Franses, Colloids Surf. **100**, 1 (1995).
[13] C. D. Eggleton and K. J. Stebe, J. Colloid Interface Sci. **208**, 68 (1998).
[14] L. Ting, D. T. Wasan, and K. Miyano, AIChE. J. **107**, 352 (1985).
[15] O. A. Ladyzhenskaya, *The Mathematical Theory of Viscous Incompressible Flow* (Gordon and Breach, New York, 1969).
[16] C. Pozrikidis, *Boundary Integral and Singularity Methods for Linearized Viscous Flows* (Cambridge University Press, Cambridge, 1992).
[17] D. Barthes-Biesel and A. Acrivos, J. Fluid Mech. **61**, 1 (1973).
[18] B. J. Bentley and L. G. Leal, J. Fluid Mech. **167**, 241 (1986).
[19] C. D. Eggleton, Y. P. Pawar, and K. J. Stebe, J. Fluid Mech. **385**, 79 (1999).
[20] Y. T. Hu, D. J. Pine, and L. Gary Leal, Phys. Fluids **12**, 484–489 (2000).